Ultrafast thin-disk multipass laser amplifier scheme avoiding misalignment induced by natural convection of the ambient air

Christoph Röcker
Jan-Philipp Negel
André Loescher
Tom Dietrich
Stefan Piehler
Benjamin Dannecker
Thomas Graf
Marwan Abdou Ahmed

Ultrafast thin-disk multipass laser amplifier scheme avoiding misalignment induced by natural convection of the ambient air

Christoph Röcker,[*] Jan-Philipp Negel, André Loescher, Tom Dietrich, Stefan Piehler, Benjamin Dannecker, Thomas Graf, and Marwan Abdou Ahmed
Universitaet Stuttgart, Institut fuer Strahlwerkzeuge, Laser Development, Stuttgart, Germany

Abstract. We report on an approach for a compact ultrafast thin-disk multipass laser amplifier making use of a highly compact geometric folding scheme. The setup is also suitable to minimize the effects caused by natural convection of hot air in front of the thin-disk on the amplified laser beam as it facilitates to orient the laser disk with its axis in the vertical direction. The efficacy of this approach is analyzed with finite-element method simulations of the heated laser crystal in ambient air with different orientations of the thin laser disk. The experiments confirm a significant improvement of the amplifier performance in terms of stability and an increase of the output power with nearly diffraction-limited beam quality ($M^2 \leq 1.4$) by a factor of 3 with respect to the conventional orientation of the laser disk. © *The Authors. Published by SPIE under a Creative Commons Attribution 4.0 Unported License. Distribution or reproduction of this work in whole or in part requires full attribution of the original publication, including its DOI.* [DOI: 10.1117/1.OE.58.9.096102]

Keywords: lasers; laser amplifiers; ultrafast lasers; thermal effects.

Paper 190732 received May 27, 2019; accepted for publication Aug. 14, 2019; published online Sep. 11, 2019.

1 Introduction

Laser material processing with ultrashort laser pulses has been a rapidly growing field in recent years. Several promising applications demand high average power in order to increase productivity as well as for high pulse energies to allow for multispot parallel processing.[1] In particular, processing at low repetition rates in the range of several tens of kilohertz is promising since thermal damage induced by heat accumulation caused by consecutive pulses can be effectively avoided.[2,3] By now, several laser architectures are suited to deliver average power in the kW range.[4–8] Due to the completely passive approach, the low number of transmissive optics, and the possibility to scale the beam diameter to reduce nonlinear effects, the thin-disk based multipass amplifier (TDMPA) scheme is a promising architecture to reach very high output power and energy.[9–12] However, due to the deflection of the laser beam, which is caused by the heated ambient air in front of the surface of the pumped laser crystal by natural convection (referred to as "air-wedge" in the following), the output power that can be achieved in the TDMPA architecture is limited to a few hundreds of watts, if no compensating element is used, such as introduced in Ref. 11. In contrast to thin-disk based regenerative amplifiers, which are based on a cavity and therefore can be realigned with the end mirror to compensate for pump power-dependent misalignment, the realignment of a TDMPA during high power operation is particularly critical due to the long propagation length of the signal beam in the amplifier. To maintain the alignment of the beam path, the TDMPA architecture, therefore, relies on passive compensation strategies. For this reason, state-of-the-art TDMPAs require a retroreflecting mirror pair (RMP) in order to minimize the deflection of the laser beam caused by the air-

wedge effect.[11] But even with the RMP, residual pump power-dependent air-wedge induced misalignment is usually observed. Other approaches, such as the operation in vacuum or a helium atmosphere, demonstrated to reduce thermo-optical wavefront aberrations in an oscillator and should also be applicable to TDMPAs but increase the complexity of the overall system.[13,14] For laser resonators operating in continuous wave, a passive compensation based on a grating end mirror in Littrow configuration has been successfully demonstrated.[15] But as this concept requires the feedback of a resonator to allow for a shift in the oscillating wavelength to correct for an air-wedge induced change of the angle of incidence on the grating, this approach cannot be applied to TDMPAs. Another common approach to reduce the pump power-dependent misalignment caused by the air-wedge effect is the reduction of the temperature of the laser crystal by reducing the heat generated during the pumping process of the laser active medium. This is accomplished by a reduction of the quantum defect by pumping directly in the upper laser level, which is usually referred to as "zero phonon line pumping (ZPL)."[11,14,16–19] For Yb:YAG-based systems, the pump spectrum, in this case, needs to be locked to 969 nm (~3 nm FWHM) instead of 940 nm (~15 nm FWHM).[17] Although ZPL significantly reduces the heat load, it can neither completely avoid heating of the laser crystal nor the resulting thermally induced effects.

In this paper, we report on an ultrafast thin-disk multipass laser amplifier in which the misalignment effects caused by the heated air in front of the pumped thin-disk crystal are mitigated by orienting the disk with its axis in vertical direction. The efficacy of the approach was proven by comparing the same amplifier with the thin laser disk mounted in two different orientations and showed that the setup with the disk facing downward allows to reach a higher output power with an improved beam quality and stability of the output power and pointing of the laser system without the necessity for any

*Address all correspondence to Christoph Röcker, E-mail: christoph.roecker@ ifsw.uni-stuttgart.de

compensating optical elements, such as the RMP even without resorting to ZPL-pumping or operation in a different ambient gas.

2 Simulation of Natural Convection at the Thin-Disk Crystal

In order to model the optical effects of natural convection on the laser beam, we used the finite-element method in COMSOL-Multiphysics to simulate the heated laser crystal in ambient air. The model comprises the heat transfer in solids to model the temperature distribution in the optically pumped thin disk and fluid dynamics to simulate the heat transfer due to natural convection and the flow of the ambient gas. The change of the refractive index of the ambient gas was determined based on the calculated temperature distribution in the air. The temperature dependence of the refractive index of air
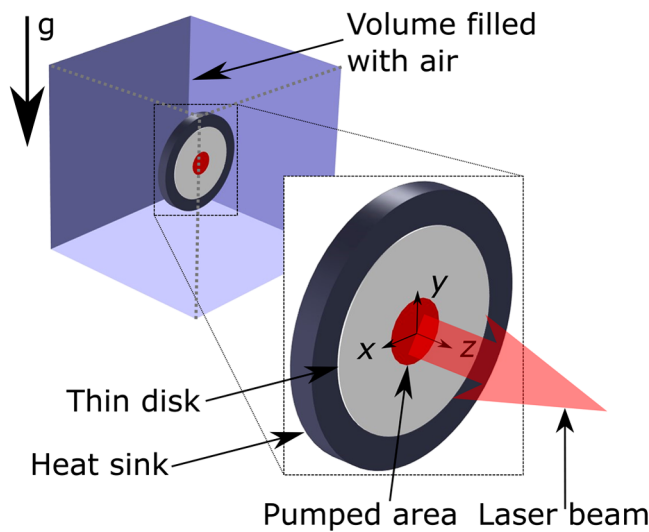

Fig. 1 Schematic illustration of the thin disk in its conventional orientation facing in horizontal direction (configuration *H*). The arrow marked "g" indicates the direction of gravitational acceleration, which determines the direction of convection. The surface normal of the laser crystal coincides with the propagation axis of the laser beam (*z* axis).

at a wavelength of 1030 nm was taken into account by $n_{Air} = 1 + 2.83707 \cdot 10^{-4} - 7.88613 \cdot 10^{-7} \cdot T$, where T is the temperature of the air in °C. This formula was obtained by a linear fit of the data given in Ref. 20. An atmospheric pressure of 1 atm and a relative humidity of 20% were assumed. To illustrate the optical effect of the heated air on an incident laser beam, the distribution of the refractive index is then used to calculate the varying optical path lengths (OPLs).

The simulations were carried out assuming a thin disk with a thickness of 110 μm and a diameter of 15 mm. The optically pumped region was modeled as a circular area on the surface of the disk with a constant temperature of 80°C. The disk is mounted on a 2-mm thick diamond heat sink with a diameter of 20 mm. The thermal contact between the heat sink and the thin-disk is assumed to be ideal. The cooling was modeled by a constant temperature of 17°C on the backside surface of the diamond heat sink. The thin-disk on the heat sink is located in the center of a $40 \times 40 \times 40$ mm^3 cube of air, which has open boundaries to all sides. In order to model the buoyancy caused by natural convection, a volume force was defined that is acting on the gas volume. This volume force depends on the mass density, which in turn depends on the temperature of the gas, and can be expressed as $f_v = F/V = \rho * g$, with the force F, the volume V, the gravitational acceleration $g = 9.81$ m/s^2 and the density of the gas ρ.

As illustrated in Fig. 1, usually, the thin-disk is implemented with its surface normal oriented perpendicularly to the gravitational acceleration and the laser beam incident in the horizontal direction (referred to as horizontal configuration *H* in the following). According to the coordinate system shown in the figure, the gravitational acceleration is oriented in the direction $-y$ and the laser beam axis is parallel to the z axis.

For this configuration *H*, Fig. 2 shows two cross sections of the calculated temperature distribution in the ambient air. The temperature distribution in the vertical (*y-z*) plane is shown in Fig. 2(a) and the one in the horizontal (*x-z*) plane in Fig. 2(b). As can be seen in Fig. 2(a), due to the natural convection, a temperature gradient in the direction of the
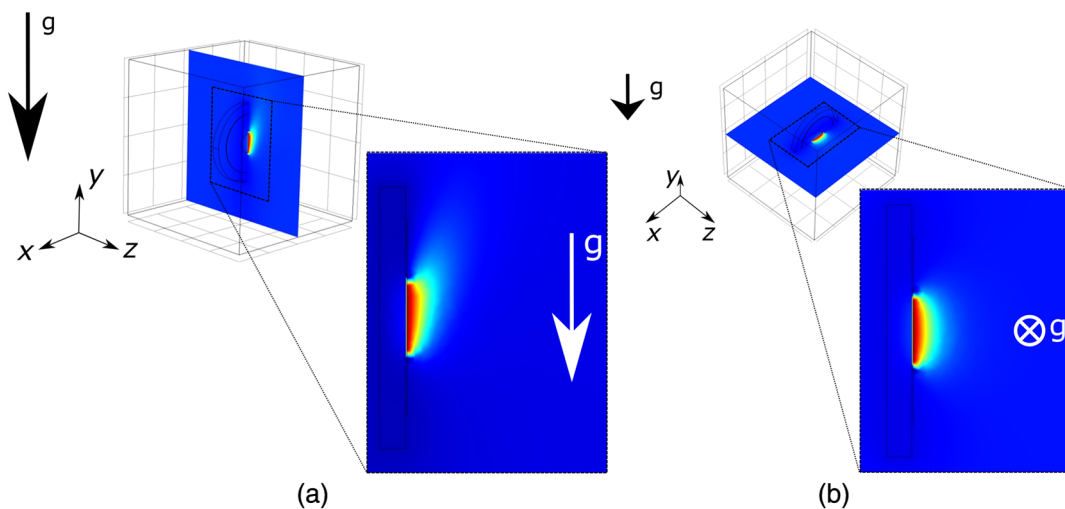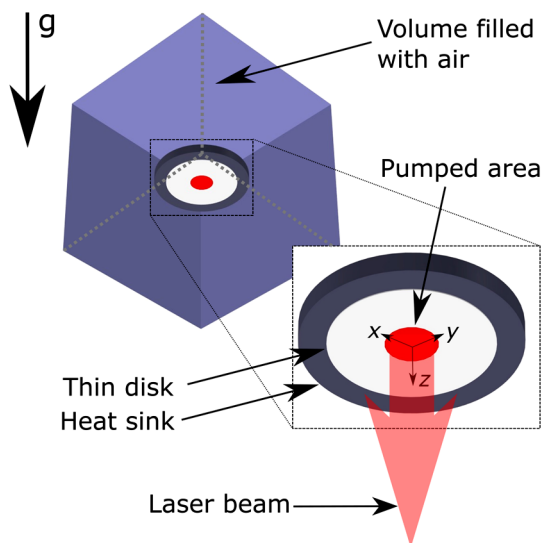

Fig. 2 Distribution of the temperature of the ambient air (a) in the vertical (*y-z*) and (b) in the horizontal (*x-z*) sectional plane for configuration *H*.

gravitational acceleration is observed. This gradient causes, with respect to the axis of the laser beam (z-axis), an asymmetric temperature distribution in the vertical plane. In contrast, the temperature distribution in the horizontal plane, shown in Fig. 2(b), is symmetric with respect to the axis of the laser beam.

Due to buoyancy, the gravitational acceleration determines the direction of the natural convection and with it the direction of the temperature gradient in the ambient air. When mounting the thin-disk with its surface normal in a direction parallel to the gravitational acceleration instead, the direction of natural convection and with it the temperature gradient occur parallel to a vertically incident laser beam. The z axis is now vertically oriented in the direction of the gravitational acceleration, as shown in the sketch of this arrangement in Fig. 3 (referred to as vertical configuration V in the following).

The temperature distribution in the ambient air for a disk mounted in configuration V is shown in Fig. 4(a) for the y-z plane and Fig. 4(b) for the x-z plane, respectively. In contrast to the situation in configuration H, the temperature distribution is now found to be almost rotationally symmetric with respect to the axis of the laser beam.

To further illustrate the difference between the beam distortions induced by the two different configurations, Fig. 5
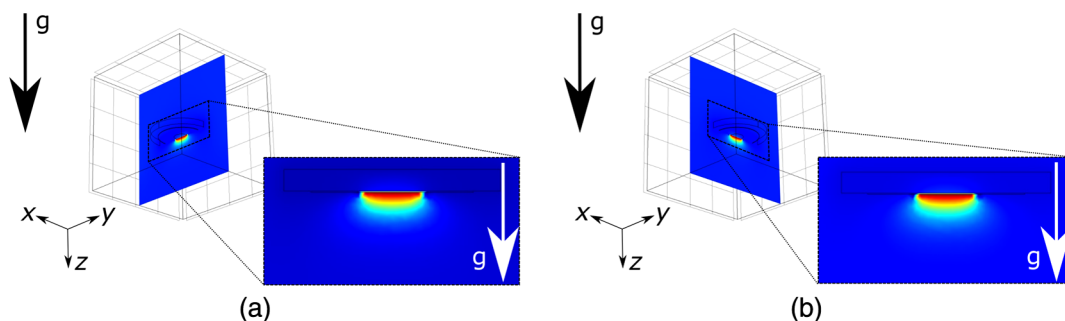
shows the varying OPL occurring in the y-z [Fig. 5(a)] and the x-z [Fig. 5(b)] sectional planes for both configurations, whereas the pumped area is centered at $x = y = 0$.

Due to the thermal dispersion of air, a change of the temperature results in a change of the OPL. While a constant OPL across the beam only leads to an overall phase delay, a linear variation of the OPL across the beam causes an angular deflection of the beam. As depicted in Fig. 5(a), the temperature distribution in the y-z plane of configuration H results in a linear variation of the OPL (illustrated by the black dashed line), which leads to angular deflection of the beam in the vertical direction. In contrast, the distribution of the OPL occurring in configuration V is symmetric and therefore does not lead to angular deflection of an incident beam. Hence, when the laser crystal is oriented to face in the vertical direction (configuration V), the lateral misalignment of the beam can be avoided.
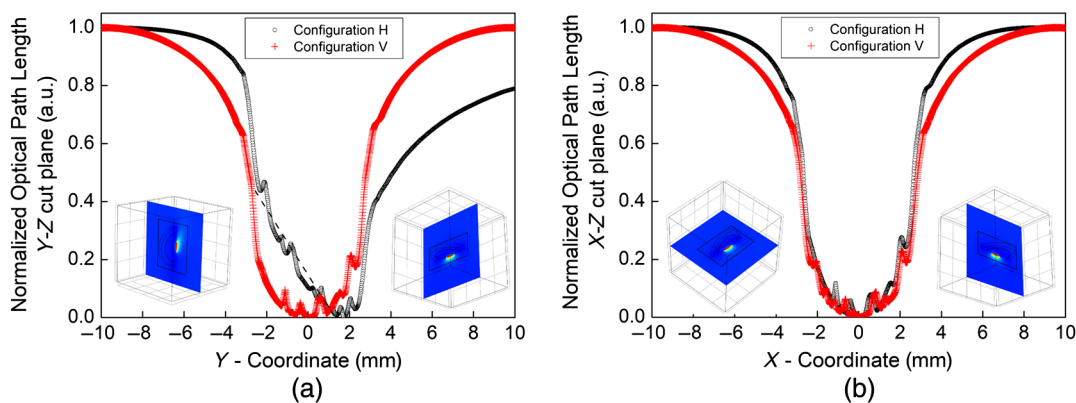
This advantage of orienting the thin disk facing in a vertical direction was confirmed also by experimental investigations, as reported in the following sections. The experiments were carried out with a geometric folding scheme of the TDMPA, which allows for more compact setup. While it was not designed to be operated at power beyond the order of 100 W, it was yet suitable to compare the two above discussed configurations and demonstrate the efficacy to improve the performance of the amplifier by orienting the thin-disk laser facing in vertical direction.

3 Experimental Setup

The seed laser used in our experiments emitted 6.5-ps long pulses (FWHM, assuming a Gaussian temporal shape) at a central wavelength of 1030 nm. It was operated with a repetition rate of 30 kHz. The available average power was limited to 11 W. The beam propagation factor was $M^2 < 1.2$.

The thin-disk laser crystal used in the amplifier was a 11 at.% Yb:YAG disk with a diameter of 12 mm and a thickness of 110 μm, glued on a diamond heat sink. The diameter of the pumped area on the disk was ~4.8 mm. The radius of curvature of the disk was ~20 m concave. The crystal was placed in a 24-pass pump module and pumped at a central wavelength of 940 nm. The pump module used in this experiment is not sealed on the backside to avoid trapping of hot air in the module.

The side view of the amplifier is schematically illustrated in Fig. 6, and the beam path of the whole experimental setup is depicted in Fig. 7. To fold the beam path multiple times over the thin-disk crystal, a new rotationally symmetric arrangement was used, comprising 30 adjustable plane high-

Fig. 3 Schematic illustration of the thin disk mounted in the vertical configuration V. The axis of the laser beam is parallel to the gravitational acceleration.

Fig. 4 Distribution of the temperature of the ambient air in the (a) y-z and (b) x-z sectional plane for a disk mounted in configuration V.

Fig. 5 (a) Calculated distribution of the OPL in the y-z (a) and the x-z (b) plane. The pumped area is centered at $x = y = 0$ and extends to ± 2.4 mm. The insets indicate the corresponding planes, as shown in Figs. 2 and 4.
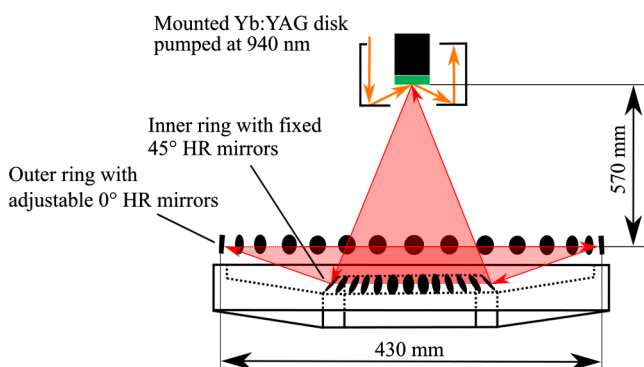
Fig. 6 Concept of the compact multipass amplifier. The beam path of the pump and seed beam is indicated by orange and red arrows, respectively. The HR mirrors (AOI 45 deg) mounted in the inner ring unfold the solid angle onto the outer ring, where HR mirrors (AOI 0 deg) are mounted in adjustable mirror holders to fold the beam multiple times over the thin-disk.

reflective (HR) mirrors for an angle of incidence (AOI) of 0 deg on an outer ring and another 30 fixed plane HR mirrors (AOI 45 deg) on an inner ring. The compact footprint is achieved by using the inner ring of mirrors to unfold the solid angle onto the outer ring of mirrors. In the present setup, the diameter of the outer ring is 430 mm and the distance between the plane with the outer ring of folding mirrors and the thin-disk laser crystal is 570 mm. Accordingly, the overall beam path length is significantly reduced as well compared to the previous TDMPA[9–12] since no additional folding optics in the vicinity of the thin-disk [mirrors M1, M(20–21), M(40–41), RMP] are required to fold the beam to different positions on the mirror array.

The propagation of the seed beam through the amplifier is based on a quasi-collimated free-space-propagation scheme, as it is presented in Refs. 9–12. This scheme utilizes one or more curved optics in each pass (typically the thin-disk) inside the multipass amplifier to counteract the beam divergence due to the propagation distance. As a result, the beam diameter does not remain constant but modulates over the propagation distance within a certain range. To enable this propagation scheme with a high overlap of the seed beam bundle and the pumped area, the linearly polarized incident seed beam is adapted to a collimated beam diameter of

~2.75 mm by means of a telescope consisting of the two curved mirrors shown in Fig. 7. The beam path through the multipass folding optics depicted in Fig. 7 follows the numbering of the optical elements: The seed beam first reaches (the adjustable) mirror 1, where it is reflected toward (the fixed) mirror 2 in the inner ring. Mirror 2 is oriented in such a way that the beam is reflected onto the center of the thin-disk laser crystal. After a reflection from the backside of the disk, the beam is reflected to the fixed mirror 3 on the opposite side of the inner ring and is consequently reflected to mirror 4 on the outer ring. Mirror 4 is then used to direct the beam to mirror 5, which in turn is adjusted to reflect the beam to mirror 6. From here, the beam is again directed to the center of the thin-disk, where it is reflected toward mirror 7. This scheme is continued until mirror 59 is reached. After the reflection from mirror 59, the beam passes a quarter-wave plate and subsequently the end-mirror 60, which reflects the beam back along the same path. Hence, the beam with its polarization rotated by 90 deg propagates back through the complete system passing all the elements again in reverse order. With the present setup, one obtains a total of 30 reflections at the backside of the thin-disk laser crystal. The total length of the beam path in this multipass amplifier amounts to ~60 m. It is possible to increase the number of passes in the multipass amplifier by adding additional pairs of rings or by increasing the diameter of the rings.

In order to protect the multipass setup from dust and external airflows, the setup was housed, as indicated by the dashed line in Fig. 7. It is worth mentioning that the presented optical setup is very sensitive to pump power-dependent misalignment as the optical layout does not form nor include a passive compensation of angular deflection of the laser beam comparable to the RMP in Refs. 9–12.

4 Experimental Results

The efficacy of the strategy to orient the thin-disk laser crystal facing downward is shown in the following section by a direct comparison of the amplification results achieved in configuration H and V.

4.1 Amplification Performance

Figure 8 shows the output power and the optical efficiency of the amplifier in the two configurations H and V. The insets show the intensity distribution of the output beams. The
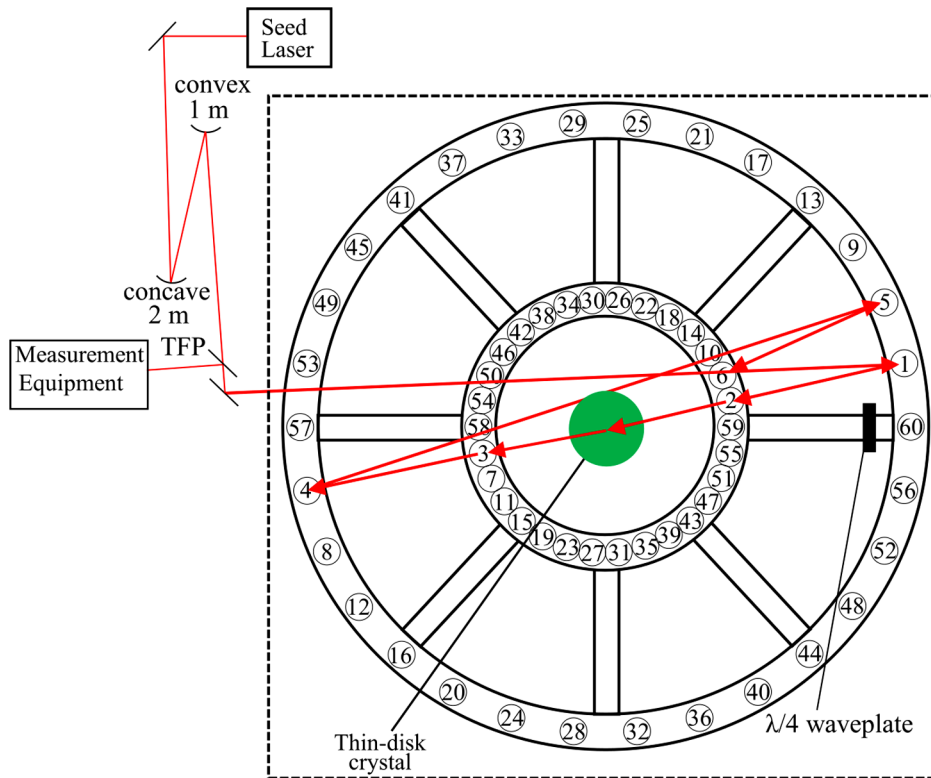
Fig. 7 Schematic top view of the experimental setup of the multipass amplifier showing the two ring arrays of mirrors and the thin-disk laser crystal. The numbering of the components indicates the order in which they are being passed by the seed laser. The amplified output beam is separated from the incident seed using a thin-film polarizer (TFP), as the polarization of the amplified beam is rotated by 90 deg by the quarter-wave ($\lambda/4$) plate in front of mirror 60. The dashed line indicates the housing of the multipass setup.
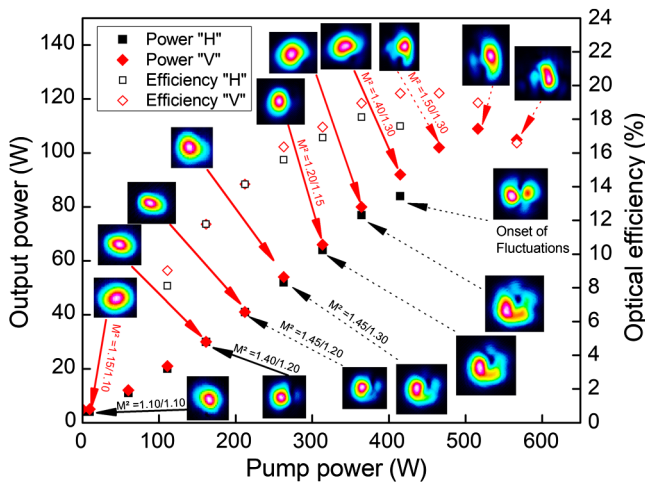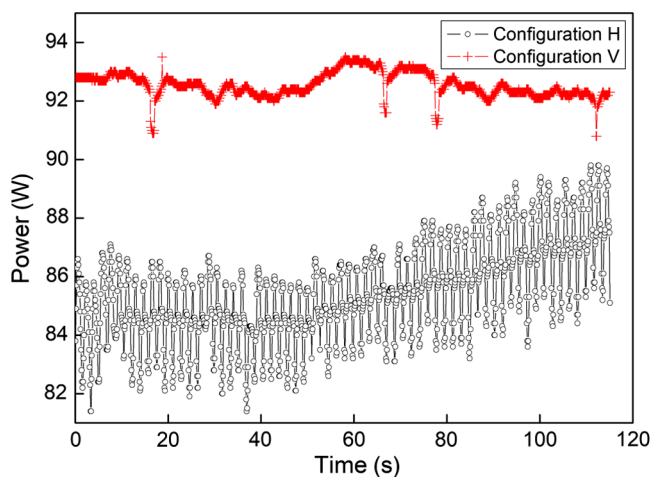

Fig. 8 Output power and optical efficiency (seed power subtracted) of the amplifier in configuration H (black) and V (red). The insets show the far-field intensity distributions of the amplified laser beam at the corresponding pump power. Solid arrow lines indicate $M^2 \leq 1.4$, while dashed arrow lines indicate $M^2 > 1.4$ in at least one transverse axis of the caustic.

numbers next to the arrows give the values of the measured M^2 (according to ISO 11146). All power measurements were performed with the same power meter, which, according to the certificate of calibration, has a relative measurement error of -0.5%. In configuration H, only 30 W of output power
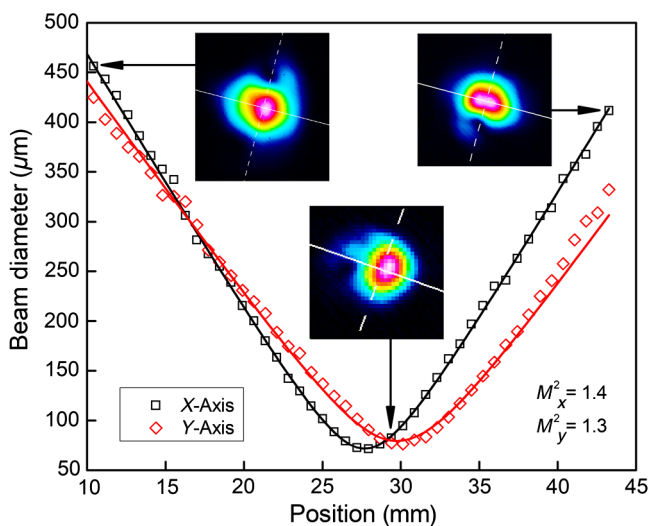
was achieved with $M^2 \leq 1.4$. With the seed power of 11 W subtracted, this corresponds to an optical efficiency of 11.8%. A further increase of the pump power led to a significant lateral displacement of the beams at the location of the disk, which was accompanied by increasingly strong distortions of the output beam's intensity profile and an increase of the $M^2 > 1.4$. This displacement of the beams on the thin-disk was observed and described also in previous publications for multipass amplifiers[11] and high power thin-disk oscillators in fundamental-mode operation.[15] Up to an output power of about 84 W, the beam in the investigated setup is only displaced and distorted but reaches a steady state at every power level within seconds. When the output power in configuration H exceeded 84 W, the beams incident on the thin disk were observed to undergo an almost periodic fluctuating movement. Due to the strong transient fluctuations in the beam intensity profile, it was not possible to obtain a reliable measurement of the M^2 in this situation and a further increase of the power was not attempted to avoid damaging the components.

The strong periodic fluctuation of the beam in configuration H also has an impact on the output power, which is illustrated in Fig. 9, where the measured output power of the two configurations at a pump power of 415 W is shown as tracked over a duration of about 120 s.
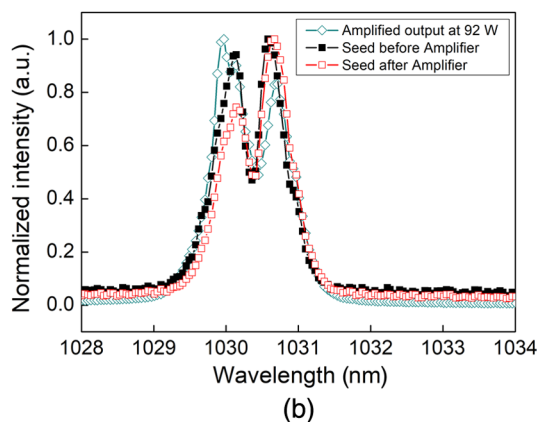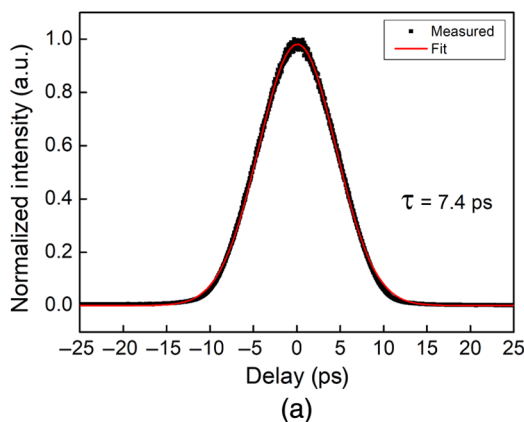
With configuration V, it was possible to achieve an output power of 92 W with M^2 still ≤ 1.4. This corresponds to 3.1 mJ of pulse energy. The M^2 was measured to be 1.4 and 1.3 in the major and minor axis, respectively. The beam

Fig. 9 Output power versus time at 415 W of pump power for operation of the amplifier in configuration H and V.

Fig. 10 Beam quality measurement at an output power of 92 W in configuration V. The insets depict the intensity distributions of the amplified beam.

caustic measured at this point of operation is shown in Fig. 10 together with the intensity distribution of the near and far field.
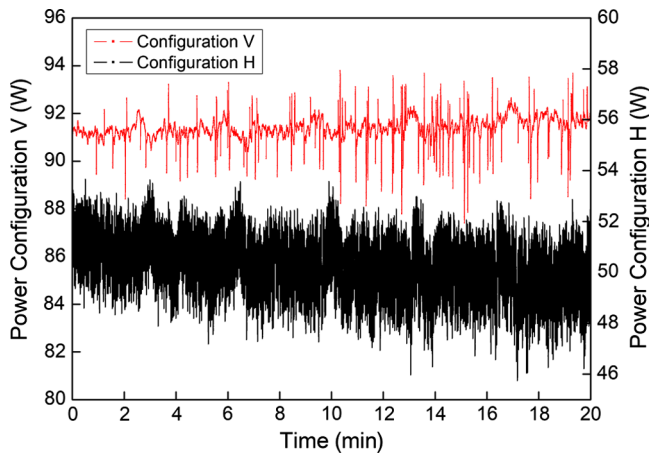
Comparing the output power that can be achieved with the same beam quality of $M^2 = 1.4$ shows that the output power achieved with configuration V is approximately three times the one obtained from configuration H.

The normalized intensity autocorrelation trace and spectrum of the pulses amplified with the configuration V are presented in Figs. 11(a) and 11(b), respectively. Assuming a Gaussian temporal profile, a pulse duration of 7.4 ps (FWHM) was measured at an output power of 92 W. This corresponds to a peak power of 0.39 GW.

The present setup with the new ring-shaped arrangement of the folding mirror was not designed for significantly higher power. At output power exceeding about 100 W, a slow lateral drift of the beams was therefore observed that set in after some minutes of operation. After switching off the pump laser, the beams returned to their initial positions within a few minutes. This long-time scale indicates that the drift is caused by thermomechanical deformations of the whole setup and not by the air-wedge effect that leads to a much faster (seconds) shift of the beams to a new position at each change of the pump power.

4.2 Long-Term Stability

The long-term power and pointing stability of configuration V were measured at an output power of 91 W. As it was not possible to operate the amplifier in configuration H at a comparable power level for a longer time, its stability performance was recorded at a pump power of 260 W, which corresponds to 50 W of output power (but $M^2 = 1.45/1.3$) for comparison. In both cases, the long-term measurement of the output power started ~20 min after setting the pump power to the specified value. The results are shown in Fig. 12. Infrequently appearing power spikes are observed for configuration V, whereas in configuration H, a strong noise with a similar magnitude is observed. The peak-to-valley deviation observed during the tracked 20 min was 7.9 and 6.4 W for configuration H and V, respectively. This corresponds to a relative power deviation of 15.7% and 7.0% for the H and the V configuration, respectively.

Fig. 11 (a) Autocorrelation trace and fit at 92 W of average output power in configuration V. From the autocorrelation trace the pulse duration was determined to be 7.4 ps (FWHM, assuming a Gaussian temporal shape). (b) Normalized spectra of the unamplified seed laser before and after the amplifier and the amplified beam at 92 W of output power in configuration V.

Fig. 12 Long-term measurement of the output power of the amplifier operated at an average output power of 91.4 W in configuration *V* and 50.3 W in configuration *H*. Measurements were carried out with the same device, sampling rate, and time intervals, respectively.
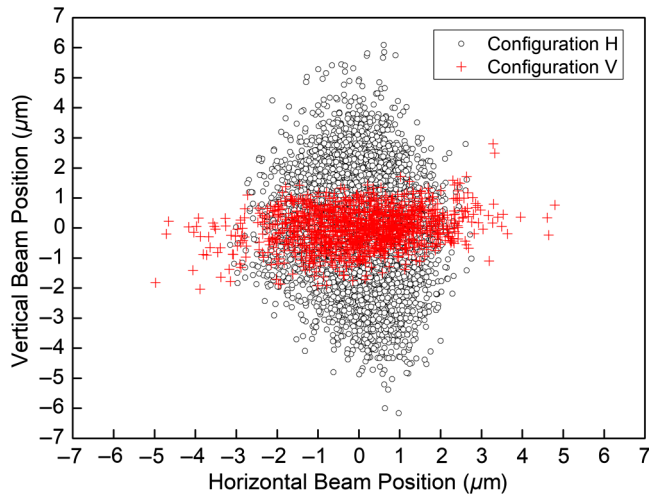
Fig. 13 Beam positions on a camera that was placed in the focal plane of a lens. The *x*-axis coincides with the horizontal direction in the laboratory system.
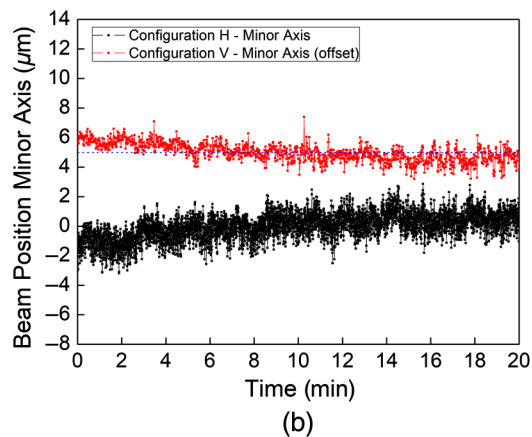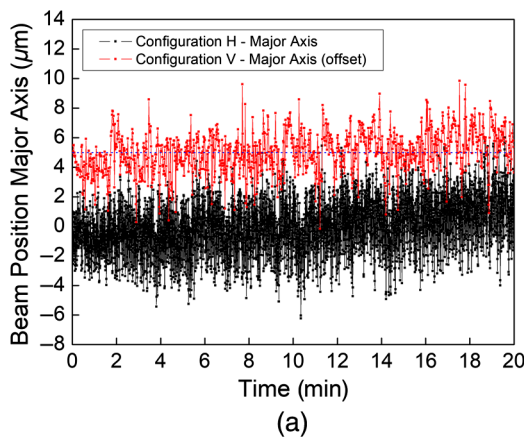
Still, for the same time interval, the standard deviation of the power was determined to be 1.25 W for configuration *H*. Normalized to the average power of 50.3 W, this corresponds to a relative power fluctuation of 2.48%. In configuration *V*, the standard deviation was found to be 0.56 W. Normalized to the average power of 91.4 W, this corresponds to 0.61%. This shows that the long-term stability of the output power of the amplifier operated in configuration *V* was significantly improved as it avoids the air-wedge effect in front of the thin laser disk. The origin of the residual power spikes observed in configuration *V* could not be determined entirely but is suspected to be related to the mechanical stability of the prototype experimental setup.

To compare the long-term performance of the amplifier in terms of beam pointing stability (according to DIN EN ISO 11670), a camera was placed in the focal plane of a lens with a focal length of $f_{\mathrm{Lens}} = 100$ mm. To reduce influences of the ambiance, the camera was located close to the output of the amplifier at a distance of ∼50 cm from the TFP of the amplifier. The measurement was performed at the same time as the long-term measurement of the output power presented in Fig. 12. The results of the measurements are shown as a point distribution in Fig. 13. The temporal evolution of the beam's position as evaluated along the major/minor axis of this distribution is shown in Figs. 14(a) and 14(b). According to DIN EN ISO 11670, the angular stability $\delta\alpha$ is characterized by $\delta\alpha_{x,y} = 2\frac{s_{\vartheta x,y}}{f}$, where f_{Lens} is the focal length of the used lens and $s_{\vartheta x,y}$ is the standard deviation in the major and minor axis of the distribution of the recorded beam positions, respectively. For operation in configuration *H*, the angular stability $\delta\alpha$ was 18.1 μrad in the minor axis and 36.1 μrad in the major axis. Operated in configuration *V*, the angular stability of the amplifier was 12.4 μrad in the minor axis and 28.0 μrad in the major axis. Compared to configuration *H*, this corresponds to a reduction of more than 22% in the major and 31% in the minor axis.

5 Conclusion

At pump power below 200 W, the amplification performance (output power and efficiency) of the multipass thin-disk laser amplifier was observed not to depend on whether the thin

Fig. 14 Beam positions on a camera chip in dependence of the time for the major (a) and minor (b) axis of the distributions shown in Fig. 13. For improved illustration, an offset of 5 μm was added to the data of configuration *V* in both plots.

disk is oriented in horizontal or vertical direction. At higher pump power, the performance of the amplifier operated with the disk facing downwards was significantly superior to the one with the disk facing in horizontal direction, not only with respect to output power and efficiency but also in terms of power stability and pointing stability. Comparing the output power that can be reached at reasonably good beam quality of $M^2 \leq 1.4$, a vertically facing disk is also clearly superior and allows to reach a power of three times the one possible with a horizontally oriented axis of the disk. With the disk facing downward, the power stability of the amplifier was improved by more than a factor of 2, whereas the pointing stability was improved by more than 20% at almost twice the output power.

In conclusion, these results show that the performance of a multipass thin-disk amplifier can significantly be improved by orienting the thin-disk laser crystal with its axis in a vertical direction to avoid a beam misalignment caused by convection of the hot air in front of the pumped thin-disk laser crystal.

Future work will focus on the implementation of this compensation concept for power scaling of TDMPA operated at multi kW-levels as well as a more detailed analysis of the air-wedge effect in terms of experiments and simulations.

References

1. C. Freitag et al., "High-quality processing of CFRP with a 1.1-kW picosecond laser," *Appl. Phys. A* **119**(4), 1237–1243 (2015).
2. R. Weber et al., "Heat accumulation during pulsed laser materials processing," *Opt. Express* **22**(9), 11312–11324 (2014).
3. R. Weber et al., "Processing constraints resulting from heat accumulation during pulsed and repetitive laser materials processing," *Opt. Express* **25**(4), 3966–3979 (2017).
4. T. Eidam et al., "Femtosecond fiber CPA system emitting 830 W average output power," *Opt. Lett.* **35**(2), 94–96 (2010).
5. M. Müller et al., "1 kW 1 mJ eight-channel ultrafast fiber laser," *Opt. Lett.* **41**(15), 3439–3442 (2016).
6. P. Russbueldt et al., "Compact diode-pumped 1.1 kW Yb:YAG Innoslab femtosecond amplifier," *Opt. Lett.* **35**(24), 4169–4171 (2010).
7. B. E. Schmidt et al., "Highly stable, 54mJ Yb-InnoSlab laser platform at 0.5kW average power," *Opt. Express* **25**(15), 17549–17555 (2017).
8. T. Nubbemeyer et al., "1 kW, 200 mJ picosecond thin-disk laser system," *Opt. Lett.* **42**(7), 1381–1384 (2017).
9. J.-P. Negel et al., "Ultrafast thin-disk multipass laser amplifier delivering 1.4 kW (4.7 mJ, 1030 nm) average power converted to 820 W at 515 nm and 234 W at 343 nm," *Opt. Express* **23**(16), 21064–21077 (2015).
10. J.-P. Negel et al., "Second generation thin-disk multipass amplifier delivering picosecond pulses with 2 kW of average output power," in *Lasers Congr. (ASSL, LSC, LAC)*, ATu4A.5 (2016).
11. J.-P. Negel et al., "1.1 kW average output power from a thin-disk multipass amplifier for ultrashort laser pulses," *Opt. Lett.* **38**(24), 5442–5445 (2013).
12. M. Abdou Ahmed et al., "Development of high-power thin-disk lasers: status and perspectives," Journées Nationales Des Procédés Laser Pour L'industrie (2017).
13. B. Weichelt et al., "Improving the brightness of a multi-kW thin disk laser with a single disk by an aspherical phase-front correction," *Proc. SPIE* **7721**, 77210M (2010).
14. A. Diebold et al., "Gas-lens effect in kW-class thin-disk lasers," *Opt. Express* **26**(10), 12648–12659 (2018).
15. T. Dietrich et al., "Passive compensation of the misalignment instability caused by air convection in thin-disk lasers," *Opt. Lett.* **42**(17), 3263–3266 (2017).
16. B. Weichelt et al., "Enhanced performance of thin-disk lasers by pumping into the zero-phonon line," *Opt. Lett.* **37**(15), 3045–3047 (2012).
17. T. Kasamatsu, H. Sekita, and Y. Kuwano, "Temperature dependence and optimization of 970-nm diode-pumped Yb:YAG and Yb:LuAG lasers," *Appl. Opt.* **38**(24), 5149–5153 (1999).
18. J. J. Romero et al., "Continuous-wave laser action of Yb³⁺-doped lanthanum scandium borate," *Appl. Phys. B* **80**(2), 159–163 (2005).
19. D. Sangla et al., "Highly efficient Nd:YVO₄ laser by direct in-band diode pumping at 914 nm," *Opt. Lett.* **34**(14), 2159–2161 (2009).
20. J. A. Stone and J. H. Zimmerman, "Index of refraction of air," 2004, https://emtoolbox.nist.gov/Wavelength/Edlen.asp (accessed 26 April 2019).

Christoph Röcker has received his MSc degree in photonic engineering at the University of Stuttgart in 2016. Since 2016, he has been employed at the Institut für Strahlwerkzeuge (IFSW), University of Stuttgart, as laser scientist/PhD student, where he is concerned with topics in the fields of thin-disk based high-power ultrafast laser amplifiers. Special attention is directed to the field of nonlinear optics and investigations on thermally induced effects occurring in high-power laser amplifier systems.

Tom Dietrich studied mechanical and microengineering at the University of Stuttgart with a focus on technical optics and laser technology. Since 2018, he is heading the beam shaping and diagnostics group at the Institut für Strahlwerkzeuge (IFSW) at the University of Stuttgart. His research activities include modeling, characterization and implementation of diffractive waveguide elements for laser beam shaping (intra- and extracavity applications) in kW-class high-power thin-disk lasers.

Biographies of the other authors are not available.